Electronic transport and magnetoresistance in polycrystalline and epitaxial CrO_2 nanowires

Xiaojing Zou and Gang Xiao
Department of Physics, Brown University, Providence, Rhode Island 02912, USA
(Received 21 November 2007; revised manuscript received 13 January 2008; published 15 February 2008)

We have studied and compared the electrical and magnetic behavior of sub-micron-sized polycrystalline and epitaxial chromium dioxide (CrO_2) wires, grown using a selective-area growth technique. Low-temperature transport measurements have shown that the dc resistivity of polycrystalline CrO_2 wires is strongly dependent on the linewidth. Below a critical temperature, a transition from a positive to a negative temperature coefficient of resistivity is observed, which we attribute to a competition between the scattering of the conduction electrons inside the grains and scattering across the grain boundaries. Using a simple model based on grain boundary scattering, we can separate and quantify each type of scattering, and based on this, we estimate a mean transmission probability through the grain boundaries to be on the order of 10^{-1}. Unlike polycrystalline wires, epitaxial CrO_2 wires behave in a highly metallic fashion, and a clear width-dependence is observed in the resistivity data for wires aligned along the *b* axis, but not for those aligned along the *c* axis. Furthermore, low-field magnetoresistance (MR) values have been measured as a function of magnetic fields applied both longitudinally and transversely. The results indicate that the MR behavior of polycrystalline CrO_2 wires is dominated by the shape anisotropy; however, for epitaxial CrO_2 wires, both the shape and magnetocrystalline anisotropy play important roles, and the resulting MR properties are found to be closely related to the orientation of the wire axis. By studying the MR curves, we inferred the internal magnetic domain structures in various single crystal CrO_2 wires and found that the spin-dependent transport is much stronger across a grain boundary than a magnetic domain wall.

DOI: 10.1103/PhysRevB.77.054417 PACS number(s): 62.23.Hj, 75.47.−m, 85.70.Kh, 72.80.Ga

I. INTRODUCTION

There has been growing interest in highly spin-polarized ferromagnets, a class of materials which are critical to the development of spin-related electronics (spintronics).[1,2] However, the measured spin polarization of traditional ferromagnets (e.g., Fe, Co, and Ni) is only around 40%–50%.[3] Using theoretical calculations, physicists have predicted the existence of so-called half-metallic ferromagnets (HMFs), which have an energy gap at the Fermi level E_F in one of the two spin channels and thus can exhibit 100% spin polarization. The experimental realization of truly half-metallic materials has the potential to allow major advances in spintronics, since the performance of most devices improves dramatically as the spin polarization of the metal approaches one. For example, highly spin-polarized ferromagnets enable the injection of electron spins from a ferromagnetic metal into a semiconductor with high efficiency,[4] as well as an enormous increase in the tunneling magnetoresistance ratios of magnetic tunneling junctions.[5]

This half-metallicity has been predicted for a number of materials, such as certain Heusler alloys, manganese perovskite $La_{0.7}Sr_{0.3}MnO_3$,[6] magnetite Fe_3O_4,[7] and chromium dioxide CrO_2.[8] However, the half-metallicity of most of these materials has yet to be demonstrated, with CrO_2 as the only material which has been unambiguously determined to be half-metallic. This has been established by point contact Andreev reflection (PCAR) data,[3,9] as well as spin-resolved photoelectron spectroscopy.[10,11]

Although numerous studies on the properties of chromium dioxide have been conducted in the past several years,[12–17] most of this research has been focused on continuous bulk films or micron-sized structures. Nevertheless, the magnetic behavior of these systems is closely related to a material's size and dimensionality. When the physical size of a magnetic system is reduced to dimensions comparable to, or smaller than, certain characteristic lengths (domain wall width, exchange length, spin diffusion length, etc.), unexpected and/or novel behavior is often observed.[18] Among the many different varieties of magnetic nanostructures, nanowires are attracting a great deal of attention due to their distinctive properties and potential application as ultrahigh density magnetic recoding media.[19,20]

Furthermore, the domain structures of epitaxial magnetic nanowires are found to be determined not only by the shape anisotropy but also the magnetocrystalline anisotropy.[21] Unlike conventional magnetic materials, chromium dioxide has the advantage of being made into epitaxial form easily by chemical vapor deposition. By controlling the linewidths and crystallographic orientations of single crystal CrO_2 nanowires, diverse domain structures are expected, due to the competition between the shape and magnetocrystalline anisotropy terms. This makes it possible to investigate the physics related to the domain wall and its mobility in a more efficient way. Therefore, the behavior of half-metallic chromium dioxide nanowires is of significance both in terms of understanding the fundamental physics of half-metals, and for the development of new spintronic applications.

In this paper, we present a study of the electron transport and magnetotransport properties of both polycrystalline and epitaxial CrO_2 nanowires with different linewidths and wire axis orientations. The physical mechanism behind these results will be discussed in detail.

II. EXPERIMENT

Chromium dioxide films can be grown on a rutile-phased titanium dioxide (TiO_2) substrate by chemical vapor deposi-

tion (CVD) using CrO_3 as a precursor.[22] The crystal properties of CrO_2 made in this manner are primarily dependent on the substrate. In our experiments, epitaxial CrO_2 structures were deposited on (100)-oriented single crystal TiO_2 substrates, while the polycrystalline CrO_2 elements were deposited on polycrystalline TiO_2 film, which was obtained by oxidizing a sputtered titanium film at 800 °C for one hour (the titanium film was deposited on a SiO_2-covered silicon wafer).

To make CrO_2 nanowires we have adopted a method known as the selective-area growth technique. This method utilizes the fact that during the CVD process, CrO_2 grows readily on the surface of TiO_2 but not on amorphous SiO_2.[23] The detailed fabrication process which we used has been reported previously.[21] To summarize, the TiO_2 substrate is first covered by a layer of SiO_2 (~100 nm) and then spin-coated with polymethylmethacrylate (PMMA) with a thickness of 350 nm. After baking at 185 °C for 30 min, a thin layer of chromium (~5 nm), which serves as a charge dissipator, is deposited and then patterned by electron beam lithography. After exposure, the Cr layer is chemically removed before the PMMA development. The developed PMMA is then used as an etching mask for reactive ion etching of the underlying SiO_2 layer in an CHF_3 atmosphere. Finally, the remaining PMMA is removed using acetone, and the sample is carefully cleaned in isopropyl alcohol and deionized water before loading into the oxidation furnace for CrO_2 deposition using CVD.

Due to the instability of chromium dioxide (i.e., decompose into Cr_2O_3 on the surface), we use this material itself as the contact to measure the electrical properties of CrO_2 nanowires. Furthermore, in our case, the length of the wires is fixed at 100 micron and thickness is controlled to be around 100 nm.

The transport measurements were carried out over a temperature range from 77 K to 300 K in a liquid nitrogen cryostat. Two small electromagnets are used to provide a maximum magnetic field of 3 kOe in the plane of the sample. The direct current (dc) resistance of samples was measured in a conventional four-probe configuration and the voltages were recorded by a Keithley multimeter.

III. RESULTS AND DISCUSSION

A. Polycrystalline CrO_2 nanowires

Figure 1 displays scanning electron microscopy (SEM) images of two polycrystalline CrO_2 wires with linewidths of $w=100$ nm and 1 μm, respectively. It can be observed that the polycrystalline wires are composed of many small single crystal grains with different crystal directions, and neighboring grains are separated by very thin intergrain regions (grain boundaries). Due to the additional lateral confinement from the SiO_2 sidewall, the average grain size decreases slightly with decreasing linewidth. Furthermore, because the nanowires were made using the selective-area growth technique, no postdeposition damage is introduced, as indicated by the clear crystal borders and grain facets shown in this figure.

To study the different contribution from electron scattering at grains and grain boundaries, we performed low temperature transport measurements on polycrystalline CrO_2 nanowires and the results are as follows.

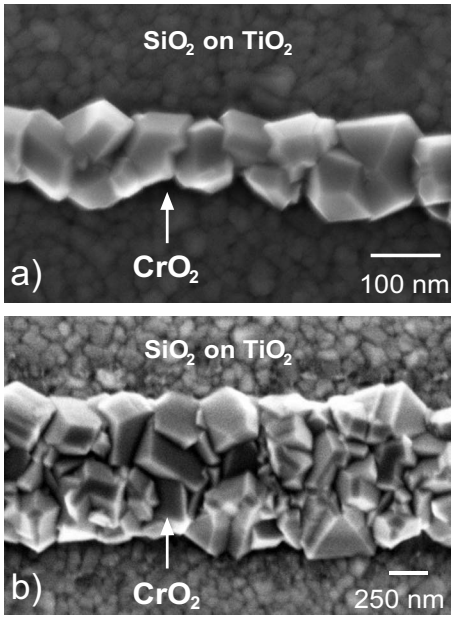

FIG. 1. SEM images of two polycrystalline CrO_2 wires with linewidths (a) $w=100$ nm and (b) $w=1$ μm. The small structures seen above and below the CrO_2 wires are polycrystalline TiO_2 nanograins covered by amorphous SiO_2.

1. Electrical properties

The temperature dependence of the resistivity $\rho(T)$ in polycrystalline CrO_2 wires with different linewidths is shown in Fig. 2. We can see that for the wire with the largest width ($w=5$ μm), the resistivity increases with increasing temperature, showing a positive temperature coefficient of

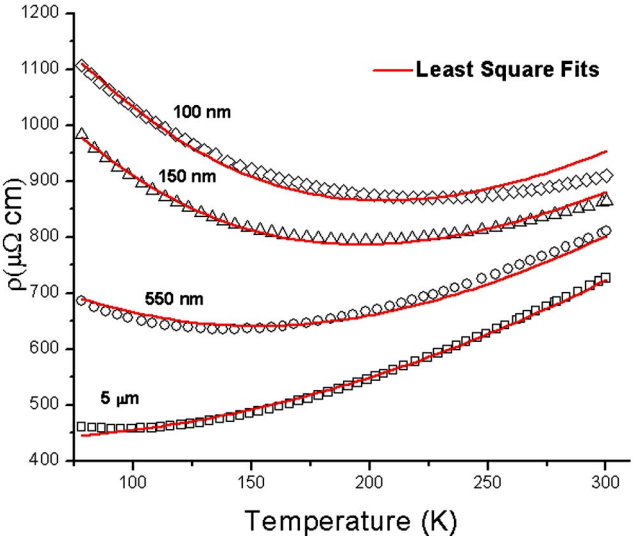

FIG. 2. (Color online) Temperature dependence of the resistivity of polycrystalline CrO_2 wires with 100 nm thickness but different linewidths. The continuous lines represent the theoretical predictions based on the grain boundary model.

resistivity (TCR), defined as $\alpha=(1/\rho)d\rho/dT$, over the full temperature range. However, for wires with smaller widths, there is a critical temperature T_m corresponding to a resistivity minimum, below which the resistivity increases with decreasing temperature, exhibiting a negative TCR. In addition, the absolute magnitude of resistivity at all temperatures increases with decreasing linewidth. To confirm the observed results and to exclude possible effects due to other factors, e.g., the decomposition of CrO_2 into Cr_2O_3, the resistance-temperature curve was measured in both directions (i.e., during heating and cooling of the sample), and the two datasets coincide very well in all cases.

The SEM results indicate that the polycrystalline CrO_2 nanograins are separated by grain boundaries. Therefore, both the electron scattering within the grains and across these grain boundaries contribute to the overall resistance of the wire. However, the resistivity of single crystal CrO_2 thin films is known to be very small, especially at low temperatures (only a few $\mu\Omega$ cm at 77 K).[13] Thus, the resistivity contribution from scattering at the interfaces between grains is likely to be increasingly important when temperature is lowered.

To explain quantitatively the grain boundary effect on the transport properties, we adopt a model proposed by Reiss *et al.*[24] A reduction in the grain size obviously leads to an increase in the density of grain boundaries, and when the grain size is comparable to the electron MFP, every grain acts like a potential well, with the interfaces functioning as energy barriers. As a result, a certain fraction of conduction electrons are localized within the well, with the measured resistivity being dependent solely on those electrons which tunnel through all the boundaries along the MFP. This effectively results in a decrease in the effective number of the conduction electrons. Therefore, the total conductivity can be written as

$$\sigma = (ne^2 l_\infty / m_e v_F) G(l_\infty, D, \Gamma), \tag{1}$$

where $ne^2 l_\infty / m_e v_F$ is the conventional Drude formula with l_∞ being the bulk MFP which describes the scattering of the electrons inside the grain, D is the mean grain dimension, Γ (<1) is the mean transmission probability of an electron through a boundary, and the total transmission function $G(l_\infty, D, \Gamma)$ reflects the influence of grain boundaries on the conductivity.

Based on some experimentally observed dependences, Reiss claimed that the reduction of the conductivity depends exponentially on the number of grain boundaries per MFP (l_∞/D). In this case, the function G can be approximated by a power law:[24]

$$G(l_\infty, D, \Gamma) \approx \Gamma^{l_\infty/D}. \tag{2}$$

Therefore, from Eqs. (1) and (2), we can express the resistivity of a polycrystalline CrO_2 thin film as

$$\rho_{\text{film}} = \rho_\infty(T)\Gamma^{-l_\infty/D} \equiv \rho_\infty(T)\exp\left[\frac{AC_0}{D\rho_\infty(T)}\right], \tag{3}$$

where $A=-\ln\Gamma$, $C_0=m_e v_F/ne^2$, and $\rho_\infty(T)=C_0/l_\infty$. The parameter C_0 is independent of temperature, and the function $\rho_\infty(T)$ represents the resistivity contribution from electron scattering inside the grains.

Generally, when the linewidth w and thickness h of a metal film are reduced down to a very small scale, the electron scattering at the film surfaces (the top and bottom surface as well as the sidewalls of a wire) introduces an extra contribution $\rho_{\text{surface}}(w,h)$ to the wire resistance, and this term is highly dependent on the ratio between the dimensions (w,h) and the electron MFP.[25,26] However, the smallest wire in our measurements has dimensions of 100 nm, which is larger than the CrO_2 electron MFP (around 30 nm at 77 K).[8] Therefore, in our case, the contribution from the surface scattering is negligible and the resistivity of a polycrystalline CrO_2 wire can be approximated from Eq. (3):

$$\rho_{\text{wire}}(w,T) \approx \rho_\infty(T)\exp\left[\frac{A(w,T)C_0}{D(w)\rho_\infty(T)}\right]. \tag{4}$$

(i) Linewidth dependence. In polycrystalline CrO_2 wires with large linewidths (a few microns or larger), each grain has several neighbors. When a current is applied, the conduction electrons take the path of least resistance by passing preferentially through the grain boundaries which have relatively high transmission probabilities. However, when the linewidth is reduced, the number of neighboring grains decreases significantly, and electrons are forced to travel along the wire axis in spite of the relative conductivity of the grain boundaries. Therefore when reducing w, the effective resistance of the grain boundaries will increase, leading to a smaller mean transmission probability $\Gamma(w,T)$ and higher $A(w,T)$ value. On the other hand, as shown in Fig. 1, the mean grain diameter $D(w)$ decreases when w is reduced. Taken together, these two effects result in the increase of $\rho_{\text{wire}}(w,T)$ for smaller linewidths at any given temperature. This dependence is consistent with our experimental data.

(ii) Temperature dependence. First, the mean transmission probability $\Gamma(w,T)$ can be assumed to be weakly dependent on the temperature, i.e., $A(w,T)\approx A(w)$, because it is most closely related to the structure of the grain boundaries. Additionally, the bulk resistivity $\rho_\infty(T)$ of a metal typically has two contributions: One is the impurity scattering term ρ_0, which is temperature independent. The other term comes from temperature dependent inelastic scattering, which scales approximately as αT^γ. Therefore, the bulk resistivity can be written as $\rho_\infty(T)\approx\rho_0+\alpha T^\gamma$.[27] The best fits to the data, based on Eq. (4) and the above two assumptions, are shown in Fig. 2 as solid lines. We can see that the agreement is good, indicating that the transport behavior of polycrystalline CrO_2 wires is well-described by the grain boundary scattering model.

The values of the fitting parameters which are listed in Table I show that the bulk resistivity $\rho_\infty(T)$ is much larger than the resistivity measured for epitaxial CrO_2 bulk films,[13] especially at low temperatures. This discrepancy can be partly attributed to the thickness dependent strain effects, which arise from the lattice mismatch between the TiO_2 substrate and the CrO_2 film.[28] The thickness of our CrO_2 sample is around 100 nm; at this value, the strain induced by the lattice mismatch is not fully released. On the other hand, for

TABLE I. Best-fit parameters, obtained from fits to the resistivity measurements of polycrystalline CrO_2 wires, as shown in Fig. 2.

Width w (nm)	100	150	550	5000
AC_0/D ($\mu\Omega$ cm)	317.4	291.5	236.1	177.2
ρ_0 ($\mu\Omega$ cm)	140.08 ± 1.52			
α ($\mu\Omega$ cm $K^{-\gamma}$)	0.0056 ± 0.001			
γ	1.98 ± 0.05			

polycrystalline CrO_2 nanowires, the stress from the SiO_2 sidewalls, which confine the lateral growth of CrO_2, may also play a role. The combination of the these effects introduces many lattice defects inside the CrO_2 nanograins and leads to a higher effective resistivity. Furthermore, during the curve fitting we assumed that $\rho_\infty(T)$ was identical for all the linewidths. However, upon reducing w, the resistivity from scattering inside the grains is likely to increase because the strain effects from the SiO_2 sidewalls increase. This probably explains that in Fig. 2 the theoretical predictions start to deviate from the experimental results for the smallest wire width (100 nm).

If we assume that the electron MFP of CrO_2 grains at zero temperature is not very different from the theoretical value predicted for large CrO_2 films, which is 70 nm,[8] the constant C_0 can thus be estimated to be $C_0 = \rho_\infty(0) l_\infty(0) \approx 9.8 \times 10^{-4}$ $\mu\Omega$ cm^2. Additionally, the mean grain size D is about 100 nm, as shown in Fig. 1. Hence, the mean transmission probability Γ can be determined to be on the order of 10^{-1}, indicating that neighboring grains are coupled with each other. We can also estimate the resistivity $\rho_{surface}(w)$ due to surface scattering, an effect which was neglected during the curve fitting. The effects of element geometry on the resistivity of a metal thin film were discussed by Fuchs and Sondheimer, and their conclusion, summarized as the FS model, was that the surface resistivity can be approximated as[25,26]

$$\rho_{surface}(w) = \frac{3}{8}(1-P)\rho_\infty(T) l_\infty(T)\left[\frac{1}{w} + \frac{1}{h}\right], \qquad (5)$$

where P represents the fraction of electrons elastically reflected by the surfaces, and h is the thickness of the sample

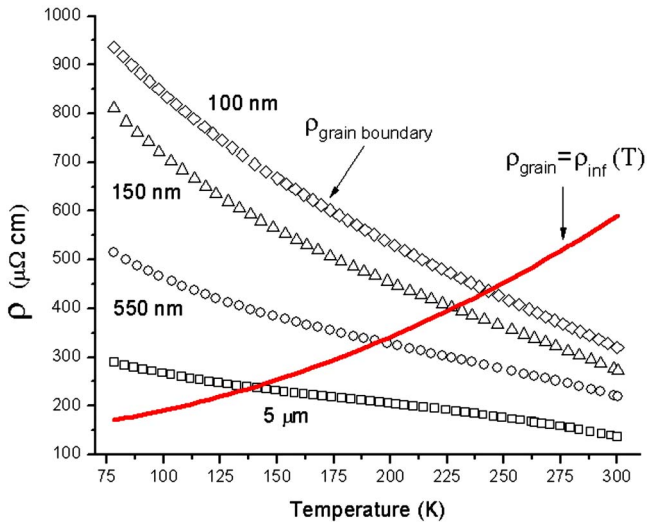

FIG. 3. (Color online) Temperature dependence of the grain boundary resistivity (open markers) and resistivity from scattering within the grains (solid line) for polycrystalline CrO_2 wires with different linewidths.

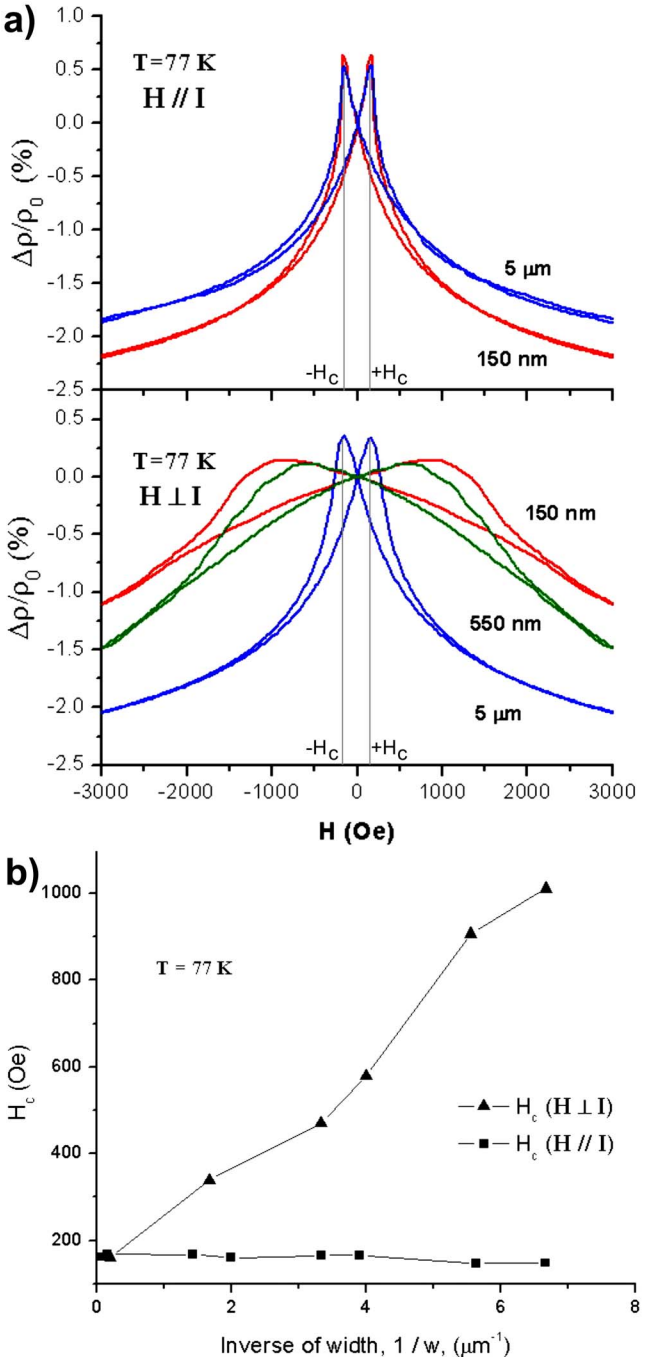

FIG. 4. (Color online) (a) Longitudinal and transverse magnetoresistance curves measured at 77 K, as a function of magnetic field H for polycrystalline CrO_2 wires with different linewidths, and (b) the coercive field H_c as a function of the inverse wire width $(1/w)$ in the longitudinal and transverse geometries for polycrystalline CrO_2 wires.

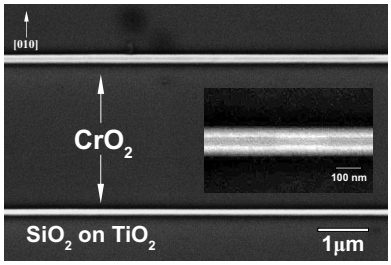

FIG. 5. SEM image of two single crystal CrO_2 nanowires grown on a (100)-TiO_2 substrate. The linewidths of the wires are 100 nm and 200 nm, respectively. The inset shows the enlarged view of the nanowire with 100 nm in width.

(100 nm). If we assume, as a worst-case scenario, that P is equal to zero, and $\rho_\infty(T)l_\infty(T)=C_0$, then $\rho_{\text{surface}}(w)$ is calculated to be 37 $\mu\Omega$ cm for $w=5$ μm and 74 $\mu\Omega$ cm for $w=100$ nm. These values are more than one order smaller than the total wire resistivity, showing that the decision to neglect the surface scattering contributions was reasonable and consistent with the experimental results.

Figure 3 displays the temperature dependence of the grain boundary resistivity and the grain resistivity $\rho_\infty(T)$ of polycrystalline CrO_2 wires with various widths. The direct contribution from the grain boundaries is determined by subtracting the grain resistivity from the resistivity of the whole wire:

$$\rho_{\text{grain boundary}}(w,T) = \rho_{\text{wire}}(w,T) - \rho_\infty(T). \tag{6}$$

It is clear that upon reducing the temperature, or the sample linewidth, the electron scattering probabilities at the grain boundaries increase greatly, as a result of an increased number of grains per electron MFP.

The temperature coefficient of resistivity can be calculated by taking the derivative of the logarithm of Eq. (4), where again $\Gamma(w)$ is assumed to be temperature independent:

$$\text{TCR} = \frac{d\ln\rho_{\text{wire}}}{dT} = \frac{d\rho_\infty(T)}{\rho_\infty(T)dT}\left(1 - \frac{A(w)C_0}{D(w)\rho_\infty(T)}\right). \tag{7}$$

Since $d\rho_\infty(T)/dT$ is always positive, the above formula indicates that a resistivity minimum occurs when $\rho_\infty(T)$, $D(w)$ and $A(w)$ fulfill the following condition:

$$\rho_\infty(T_m) = A(w)C_0/D(w). \tag{8}$$

We can see that the critical temperature T_m increases when the linewidth w is reduced. At high temperature, where $T>T_m$, the positive TCR value indicates that the scattering from electron inside the grains is the dominant contribution to the wire resistance. However, upon reducing the temperature below T_m, the grain boundary scattering gradually dominates, and thus a negative TCR value is observed. These conclusions are consistent with the data shown in Fig. 3.

2. Magnetoresistance properties

Low-field magnetoresistance (MR) results are presented in Fig. 4(a), plotted in terms of the percentage $\Delta\rho/\rho_0 = [\rho(H)-\rho_0]/\rho_0$ versus the applied magnetic field (0–3 kOe)

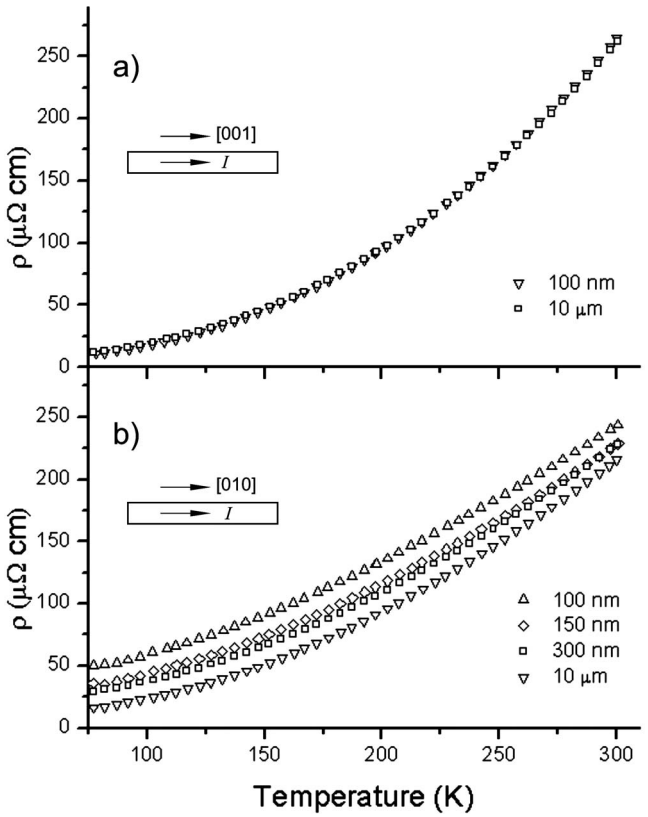

FIG. 6. Resistivity as a function of temperature for epitaxial CrO_2 nanowires with different linewidths aligned along the (a) [001] direction and (b) [010] directions. All the wires have a thickness of ~100 nm.

for polycrystalline CrO_2 wires with different linewidths. Figure 4(b) displays the linewidth dependence of the field at which each sample experiences its maximum resistivity. For polycrystalline samples, these field values are equal to the coercive field H_c for each wire.[13] We will discuss the longitudinal and transverse magnetoresistance data separately in the following.

(i) Longitudinal magnetoresistance. It is observed from Fig. 4(a) that the magnitude of MR increases when there is a reduction in the linewidth of the sample. As has been discussed previously, the mean transmission probability $\Gamma(w)$ decreases with a reduced w due to the fact that the further restriction in the available electron conduction paths causes an increase in the effective grain boundary resistance. Also, it has been reported that annealing the polycrystalline CrO_2 sample in the air increases its magnetoresistance and resistivity, which has been attributed to the partial reduction of CrO_2 into Cr_2O_3 in the grain boundary regions.[29] Thus, it seems clear that the MR value is closely related to the structure of the grain boundaries, with the MR value increasing for smaller $\Gamma(w)$, which is a direct consequence of reducing the linewidth w.

(ii) Transverse magnetoresistance. The H_c in this case shows a much stronger width dependence, following a $1/w$ law. This is due to the fact that in magnetic nanowires with linewidths w comparable to their thickness t, the demagnetizing field H_d becomes important. In the transverse case, H_d

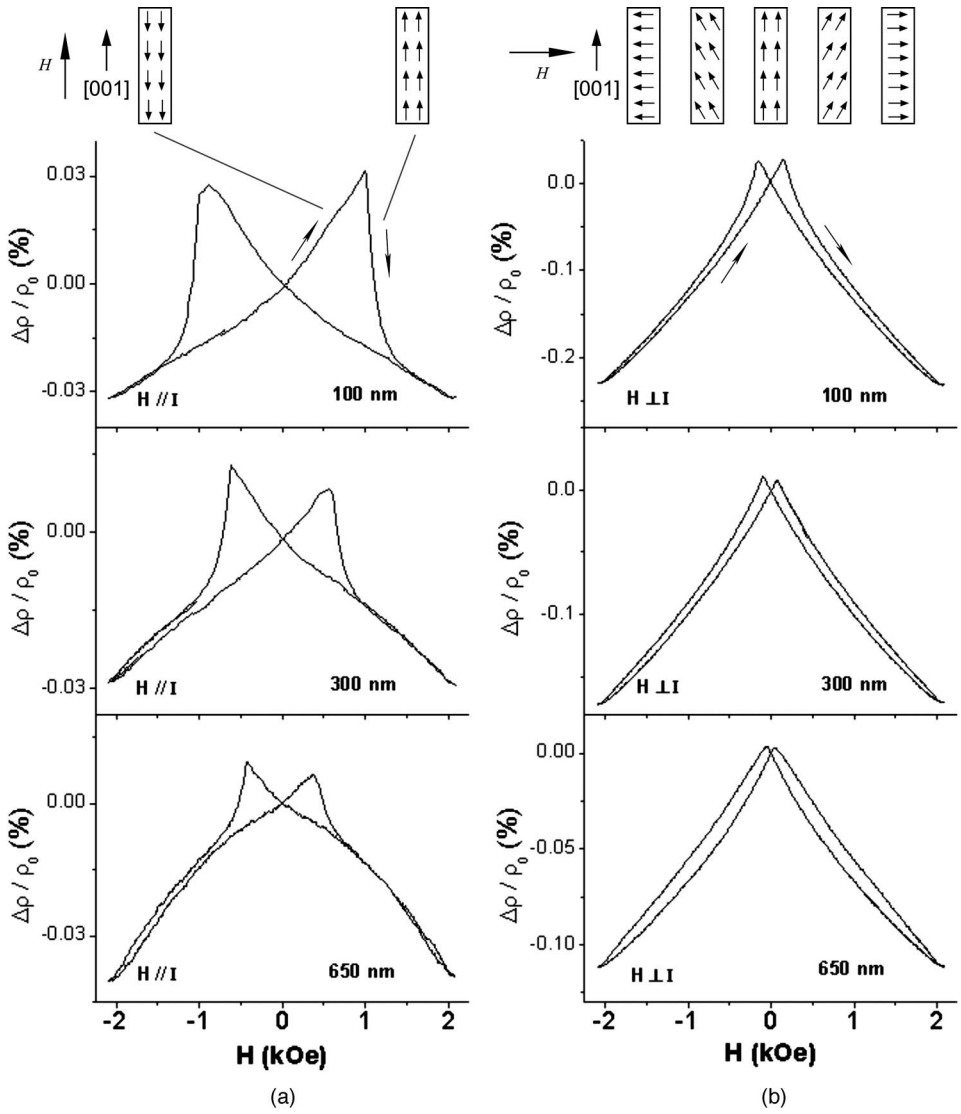

FIG. 7. Low-field (a) longitudinal and (b) transverse MR curves of epitaxial CrO_2 nanowires aligned along the [001] easy axis direction with different linewidths, measured at 77 K. The schematic drawings above each curve represent the different magnetization states present during the magnetization reversal process.

can be approximated as $H_d = 4\pi M_s t/w$,[30] and thus the applied field which is required to reverse the magnetization is given by $H_{ex} = H_{c(bulk)} + 4\pi M_s t/w$. Hence, the magnetization reversal process becomes much more difficult when the wire width is reduced, with the corresponding coercive field showing a $1/w$ behavior. When the external field is set to its maximum value (3 kOe), the wire's internal field decreases for samples with smaller linewidths. This means that saturating the magnetization of polycrystalline CrO_2 wires in the transverse direction is much more difficult for smaller linewidths w, resulting in a decrease in the MR value, as shown in Fig. 4(a).

Figure 4(b) also shows that for bulk polycrystalline CrO_2 films (i.e., $1/w \rightarrow 0$), the coercive fields H_c in the longitudinal and transverse directions are nearly the same. This implies that the polycrystalline CrO_2 samples are perfectly isotropic in the plane. However, for epitaxial CrO_2 samples, which will be discussed next, the in-plane coercive field is not isotropic.

B. Epitaxial CrO_2 nanowires

Figure 5 shows a scanning electron microscopy image of two epitaxial (100)-oriented CrO_2 nanowires deposited using selective-area growth technique. There are no grains or grain boundaries observed within the wires, indicating that these structures are single crystal.

The low temperature transport properties of epitaxial CrO_2 nanowires are discussed in the following.

1. Electrical properties

The temperature dependence of resistivity for single-crystal CrO_2 wires with different crystal orientations and linewidths is presented in Fig. 6. The resistivity of epitaxial wires is much lower than that of polycrystalline wires, and no resistivity minimum at T_m exists in single crystal wires. This observation further confirms that T_m in polycrystalline CrO_2 wire is due to the grain boundary effect. Because very few, if any, grain boundaries are formed in the epitaxial CrO_2

wires, the scattering probability of the conduction electrons is dramatically reduced, leading to a much smaller wire resistivity.

Furthermore, upon reducing the linewidth, we can see that for CrO_2 wires aligned along the [010] direction (b axis), the resistivity $\rho(w,T)$ increases at any given temperature. From 10 μm to 100 nm, the resistivity jumps by nearly 40 $\mu\Omega$ cm, as shown in Fig. 6. However, regardless of wire width, very small variations were observed in the resistivity plots of the wires whose long axis was parallel to the [001] direction (c axis). The resistivity increases by less than 5 $\mu\Omega$ cm from 10 μm to 100 nm in this case. For epitaxial CrO_2 films, band structure calculations have predicted a value of 3.5×10^{-5} $\mu\Omega\,\mathrm{cm}^2$ for $\rho_\infty(T)l_\infty(T)$.[8] Based on Eq. (5), we find that ρ_{surface} is less than 2.6 $\mu\Omega$ cm for w = 100 nm, a value which is much smaller than the resistivity changes shown in Fig. 6(b). Hence, again we can neglect the extra resistivity term due to the surface scattering, when considering the effects of decreasing linewidth w. We attribute this orientational resistivity behavior to the strain anisotropy in the single crystal CrO_2 wires, as explained next.

The lattice mismatch between a CrO_2 epitaxial film and TiO_2 substrate is −3.79% along the [010] axis and only 1.48% along the [001] axis. If we let CrO_2 grow freely, it has a preferential lateral growth direction along the [001] axis to achieve less lattice mismatch. For example, selective-area growth of a CrO_2 circular dot naturally deform into a rectangular shape with long side parallel to the c axis.[21] Therefore, the SiO_2 sidewall should produce much more pressure in the transverse direction, an effect which intensifies when reducing the linewidth, for the wires aligned along the b axis. Because higher sidewall pressure tends to generate more lattice defects (scattering centers) inside the CrO_2 nanowires, the resistivity of the wire aligned along the b axis can be expected to exhibit a much stronger linewidth dependence; this agrees with the data shown in Fig. 6.

2. Magnetoresistance properties

(i) Wires aligned along the [001] direction. Figure 7 plots the longitudinal and transverse MR as a function of the applied magnetic field H for epitaxial CrO_2 nanowires aligned along the [001] direction. All the measurements were made at 77 K.

It is clear that the [001] direction is the magnetic easy axis for single-crystal CrO_2 films with a thickness of 100 nm;[14] additionally, the shape anisotropy also favors a situation where the magnetic moments are aligned in this direction (along the wire axis). Thus, in the longitudinal case, we observe sharp magnetization changes in the CrO_2 nanowires, indicated by the resistance drops in Fig. 7(a). When the field is applied perpendicular to this easy axis, as shown in Fig. 7(b), the remanent magnetization state for the domains is along the c-axis direction. In this case, the magnetic moments rotate almost coherently from this direction to the b-axis direction when the magnitude of the transversely applied field is increased, resulting in a gradually decreasing resistivity without any sudden drops.

Figure 8 displays the coercive fields H_c, as extracted from the data in Fig. 7 as a function of the inverse linewidth. It is found that the H_c is roughly proportional to the inverse of width: $H_c \sim 1/w$. This behavior is in good agreement with investigations of some other ferromagnetic wires such as Co, NiFe, etc., and can be explained by considering the shape dependence of the stray field of the wire.[31,32] A decrease in linewidth increases the aspect ratio of the magnetic nanowires correspondingly, and results in a higher shape anisotropy, which makes the magnetic states parallel to the wire axis more favorable and more difficult to switch; hence, a higher coercivity H_c.

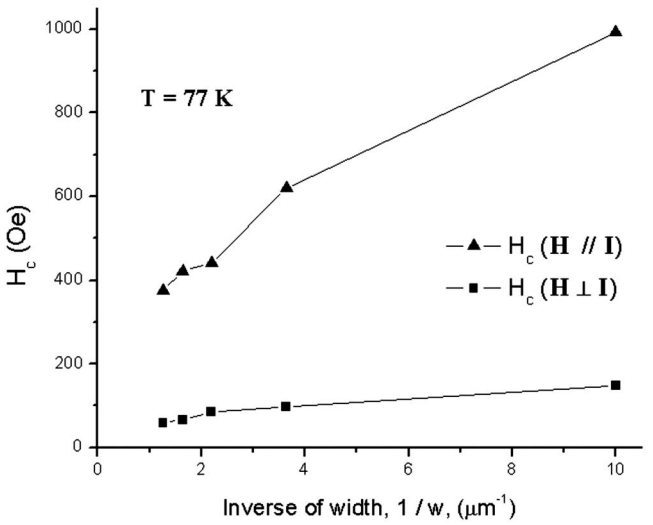

FIG. 8. Coercive field H_c as a function of the inverse linewidths $1/w$ in both the longitudinal and transverse geometries for single crystal CrO_2 wires with wire axes aligned along the [001] direction.

Unlike the polycrystalline CrO_2 bulk films, we can see that the coercive fields plotted in Fig. 8 for the two different wire geometries do not approach a single value when extrapolated to the origin. This is due to the fact that the epitaxial [001]-CrO_2 film is anisotropic within the plane because of the two distinct crystal directions. The intrinsic magnetocrystalline anisotropy favors alignment along the [001] easy axis; thus the longitudinal coercivity is larger than the transverse value, even in the limit of large linewidth.

The measured longitudinal MR properties of single crystal CrO_2 nanowires aligned along the magnetic easy axis is consistent with the observation of Konig *et al.*[15] for epitaxial CrO_2 wires with width larger than half micron. The difference in the transverse MR behaviors may lie in the different ways of fabricating CrO_2 wires. Additionally, when reducing the linewidth down to 100 nm, another MR behavior is observed for epitaxial CrO_2 wire aligned along the hard axis, which is discussed in the following.

(ii) Wires aligned along the [010] direction. In this case, the magnetic easy-axis direction, preferred by the magnetocrystalline anisotropy term, and the shape anisotropy direction are perpendicular to each other. Therefore, the magnetization behavior of the epitaxial CrO_2 wires aligned along the b axis depends on the relative strengths of these two anisotropies. Through MFM studies of epitaxial CrO_2 wires,[15,21] it has been observed that the shape dependent contribution to the anisotropy is appreciable only for CrO_2 nanowires with very small linewidths. For most of the wires, the

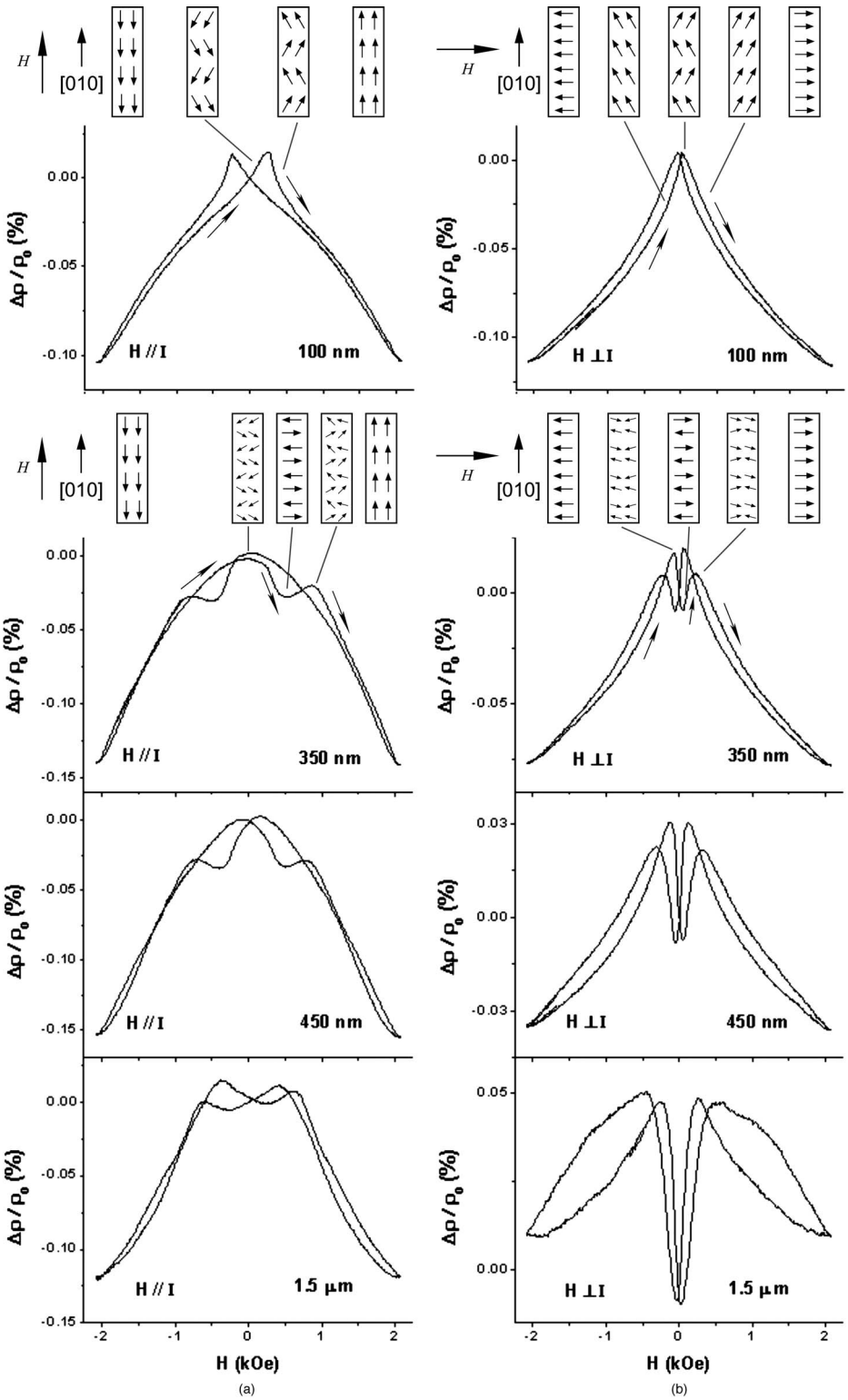

FIG. 9. Low-field (a) longitudinal and (b) transverse MR curves of epitaxial CrO_2 nanowires with different linewidths. The wires are all aligned along the [010] hard axis direction and are measured at 77 K. Schematics at the top of each figure represent the different magnetization states which occur during the reversal process.

magnetocrystalline anisotropy dominates over the shape anisotropy, giving the epitaxial CrO_2 wires a stripelike domain configuration, with domains either magnetized parallel or antiparallel to the magnetic easy axis direction ([001]) at remanence.

The magnetoresistance behavior of epitaxial CrO_2 wires along the *b* axis is shown in Fig. 9. The MR curves display more features than those [001] wires in Fig. 7. These more complex curves are the consequence of diverse types of magnetic domain patterns formed in the [010] wires. Figure 9

also shows the schematic pictures of various domain patterns at some specific magnetic states, which are inferred from the MR curves and the competitive anisotropies.

It is seen that the MR response of the smallest wire ($w=100$ nm) differs significantly from the wires with larger widths (350 nm and more). The narrowest wire exhibits MR behavior similar to that measured for wires aligned along the *c* axis, as shown in Fig. 7. This suggests that a similar magnetization reversal process exists, and the remanent magnetic state is dominated by the shape anisotropy, leaving the remanent magnetization nearly parallel to the wire axis. When the linewidth increases, the shaped-induced contribution decreases and the effects of the magnetocrystalline anisotropy become more important.

In the longitudinal case shown in Fig. 9(a) (e.g., 350 nm width), at high negative fields (−2 kOe), nearly all the magnetic moments are aligned along the wire axis, resulting in a minimal wire resistance. As the field is reduced to zero, a complicated magnetic domain structure emerges. Biehler *et al.*[16] found that, compared with the stripe domain structure obtained after initial saturating along the easy axis, this remanent state, which is formed after initial saturating along the hard axis, shows narrower domain widths because some domains do not extend across the whole wire width and the magnetization vectors in the neighboring domains are canted. Therefore, the sample resistance reaches a maximum value near zero field due to the increase in the number of domain walls.

Upon further increasing the external field in the positive direction, the stripe domain structure is formed, resulting in a lower resistance. Later on, the magnetic field is large enough to break the stable stripe domain structure, by forming extra domain walls, and this is the reason for the second resistance peak near 1 kOe in Fig. 9(a). A final decrease in the resistance is observed due to the formation, in sufficiently large fields, of a nearly single domain structure with magnetization parallel to the wire axis. A similar MR behavior has been reported recently for epitaxial CrO_2 wire with 2 μm width.[15]

In Fig. 9(b), the magnetic field is applied in the transverse direction, which is also the direction of the magnetic easy axis. At large negative applied fields, nearly all the magnetic domains are aligned in the external field direction ([001]). Upon decreasing the field value, some of the domains split into multiple smaller ones with different magnetization directions in order to minimize the total magnetic energy. In this intermediate state, the increase in domain wall scattering leads to a higher wire resistance. As the field approaches zero, these multiple domains recombine and the whole wire stabilizes in the aforementioned stripelike domain structure, which causes a reduction in the number of domain walls and leads to the resistance valley near zero field. Furthermore, we can see that this resistance valley becomes less pronounced as a wire narrows, and finally disappears for very narrow wires. This can be understood by considering that the shape-induced effects are gradually becoming important, as the linewidth is decreased, making the stripe-like domain structure, which is preferred by the magnetocrystalline anisotropy, less stable.

Overall, the magnetoresistance values measured for single crystal CrO_2 nanowires are smaller than those of polycrystalline nanowires by more than a factor of 10. This suggests that magnetic scattering at the grain boundaries is much stronger than the scattering which occurs at the domain walls.

IV. CONCLUSION

In conclusion, we have studied and compared the electrical resistivity and magnetotransport properties of both polycrystalline and epitaxial CrO_2 nanowires grown under the same conditions by chemical vapor deposition using the selective-area growth technique. A transition of the temperature coefficient of resistivity from positive to negative values is observed for polycrystalline nanowires, and the magnitude of the resistivity increases as the linewidth of the wires is reduced. Analyzing the resistivity data using a model of grain boundary scattering indicates that the bulk resistivity of CrO_2 nanograins is much larger than the values reported for single crystal CrO_2 bulk films, and this discrepancy is attributed to strain-induced defects. Resistivity measurements also show that epitaxial CrO_2 nanowires have a generally metallic character, with some anisotropy observed in the resistivity of the wires aligned along the *b*- and *c*-axis directions. When the linewidth of polycrystalline CrO_2 wires is reduced, the longitudinal MR ratio increases, due to changes in the electron conduction paths. A decrease in the transverse MR values for decreasing linewidth results from an increase in the shape-dependent demagnetizing field. Unlike the polycrystalline wires, the MR properties of single-crystal CrO_2 wires are strongly dependent on the crystal orientations of the wires, because in addition to the expected shape-induced effects, the magnetocrystalline anisotropy also plays a very important role. Our results shows that the field-dependent magnetic domain structures evolve in a complex fashion, particularly for wires that form stripelike domains at zero field. By taking advantage of the competing magnetocrystalline and shape anisotropies, one can design certain CrO_2 epitaxial nanostructures with unique magnetic domain structures, which can lead to interesting spin-dependent transport behavior.

ACKNOWLEDGMENTS

This work was supported in part by the NSF under Grant No. DMR-0605966. We also gratefully acknowledge partial support from JHU MRSEC (NSF DMR-0520491).

[1] G. A. Prinz, Science **282**, 1660 (1998).
[2] S. A. Wolf, D. D. Awschalom, R. A. Buhrman, J. M. Daughtom, S. Von Molnar, M. L. Roukes, A. Y. Chtchelkanova, and D. M. Treger, Science **294**, 1488 (2001).
[3] R. J. Soulen, Jr., J. M. Byers, M. S. Osofsky, B. Nadgorny, T. Ambrose, S. F. Cheng, P. R. Broussard, C. T. Tanaka, J. Nowak, J. S. Moodera, A. Barry, and J. M. D. Coey, Science **282**, 85 (1998).
[4] G. Schmidt, D. Ferrand, L. W. Molenkamp, A. T. Filip, and B. J. van Wees, Phys. Rev. B **62**, R4790 (2000).
[5] P. Mavropoulos, M. Lezaic, and S. Blugel, Phys. Rev. B **72**, 174428 (2005).
[6] W. E. Pickett and D. J. Singh, Phys. Rev. B **53**, 1146 (1996).
[7] A. Yanase and K. Siratori, J. Phys. Soc. Jpn. **53**, 312 (1984).
[8] S. P. Lewis, P. B. Allen, and T. Sasaki, Phys. Rev. B **55**, 10253 (1997).
[9] Y. Ji, G. J. Strijkers, F. Y. Yang, C. L. Chien, J. M. Byers, A. Anguelouch, G. Xiao, and A. Gupta, Phys. Rev. Lett. **86**, 5585 (2001).
[10] K. P. Kamper, W. Schmitt, G. Guntherodt, R. J. Gambino, and R. Ruf, Phys. Rev. Lett. **59**, 2788 (1987).
[11] Yu. S. Dedkov, M. Fonin, C. Konig, U. Rudiger, S. Senz, D. Hesse, and G. Guntherodt, Appl. Phys. Lett. **80**, 4181 (2002).
[12] K. Suzuki and P. M. Tedrow, Phys. Rev. B **58**, 11597 (1998).
[13] A. Gupta, X. W. Li, and G. Xiao, J. Appl. Phys. **87**, 6073 (2000).
[14] G. Miao, G. Xiao, and A. Gupta, Phys. Rev. B **71**, 094418 (2005).
[15] C. Konig, M. Fonin, M. Laufenberg, A. Biehler, W. Buhrer, M. Klaui, U. Rudiger, and G. Guntherodt, Phys. Rev. B **75**, 144428 (2007).
[16] A. Biehler, M. Klaui, M. Fonin, C. Konig, G. Guntherodt, and U. Rudiger, Phys. Rev. B **75**, 184427 (2007).
[17] S. T. B. Goennenwein, R. S. Keizer, S. W. Schink, I. van Dijik, T. M. Klapwijk, G. X. Miao, G. Xiao, and A. Gupta, Appl. Phys. Lett. **90**, 142509 (2007).
[18] S. D. Bader, Rev. Mod. Phys. **78**, 1 (2006).
[19] J. E. Wegrowe, D. Kelly, Y. Jaccard, Ph. Guittienne, and J. Ph. Ansermet, Europhys. Lett. **45**, 626 (1999).
[20] A. Fert and L. Piraux, J. Magn. Magn. Mater. **200**, 338 (1999).
[21] X. J. Zou and G. Xiao, Appl. Phys. Lett. **91**, 113512 (2007).
[22] X. W. Li, A. Gupta, and G. Xiao, Appl. Phys. Lett. **75**, 713 (1999).
[23] A. Gupta, X. W. Li, S. Guha, and G. Xiao, Appl. Phys. Lett. **75**, 2996 (1999).
[24] G. Reiss, J. Vancea, and H. Hoffmann, Phys. Rev. Lett. **56**, 2100 (1986).
[25] K. Fuchs, Proc. Cambridge Philos. Soc. **34**, 100 (1938).
[26] F. H. Sondheimer, Adv. Phys. **1**, 1 (1952).
[27] J. M. Ziman, *Principle of the Theory Solids*, 2nd ed. (Cambridge University Press, Cambridge, UK, 1979), Chap. 7.
[28] A. Anguelouch, A. Gupta, and Gang Xiao, IEEE Trans. Magn. **37**, 2135 (2001).
[29] H. Y. Hwang and S.-W. Cheong, Science **278**, 1607 (1997).
[30] B. Pant, J. Appl. Phys. **67**, 414 (1989).
[31] S. Y. Yuan, H. N. Bertram, J. F. Symth, and S. Schultz, IEEE Trans. Magn. **28**, 3171 (1992).
[32] K. J. Kirk, J. N. Chapman, S. Mcvitie, P. R. Aitchison, and C. D. W. Wilkinson, Appl. Phys. Lett. **75**, 3683 (1999).